Atmos. Chem. Phys., 16, 14925–14936, 2016
www.atmos-chem-phys.net/16/14925/2016/
doi:10.5194/acp-16-14925-2016
© Author(s) 2016. CC Attribution 3.0 License.

Atmospheric Chemistry and Physics Open Access EGU

Revisiting the steering principal of tropical cyclone motion in a numerical experiment

Liguang Wu[1,2] **and Xiaoyu Chen**[1]

[1]Key Laboratory of Meteorological Disaster, Ministry of Education (KLME), Pacific Typhoon Research Center (PTRC), Nanjing University of Information Science & Technology, Nanjing, China
[2]State Key Laboratory of Severe Weather, Chinese Academy of Meteorological Sciences, Beijing, China

Correspondence to: Liguang Wu (liguang@nuist.edu.cn)

Received: 30 April 2016 – Published in Atmos. Chem. Phys. Discuss.: 10 June 2016
Revised: 28 October 2016 – Accepted: 10 November 2016 – Published: 2 December 2016

Abstract. The steering principle of tropical cyclone motion has been applied to tropical cyclone forecasting and research for nearly 100 years. Two fundamental questions remain unanswered. One is why the steering flow plays a dominant role in tropical cyclone motion, and the other is when tropical cyclone motion deviates considerably from the steering. A high-resolution numerical experiment was conducted with the tropical cyclone in a typical large-scale monsoon trough over the western North Pacific. The simulated tropical cyclone experiences two eyewall replacement processes.

Based on the potential vorticity tendency (PVT) diagnostics, this study demonstrates that the conventional steering, which is calculated over a certain radius from the tropical cyclone center in the horizontal and a deep pressure layer in the vertical, plays a dominant role in tropical cyclone motion since the contributions from other processes are largely cancelled out due to the coherent structure of tropical cyclone circulation. Resulting from the asymmetric dynamics of the tropical cyclone inner core, the trochoidal motion around the mean tropical cyclone track cannot be accounted for by the conventional steering. The instantaneous tropical cyclone motion can considerably deviate from the conventional steering that approximately accounts for the combined effect of the contribution of the advection of the symmetric potential vorticity component by the asymmetric flow and the contribution from the advection of the wave-number-one potential vorticity component by the symmetric flow.

1 Introduction

The environmental steering principle has been applied to tropical cyclone track forecasting for nearly 100 years (Fujiwara and Sekiguchi, 1919; Bowie, 1922), which states that a tropical cyclone tends to follow the large-scale flow in which it is embedded. Such a steering concept has been extended to include the beta drift (also called secondary steering) that arises mainly from the interaction between tropical cyclone circulation and the planetary vorticity gradient (Holland, 1983; Chan, 1984; Chan and Williams, 1987; Fiorino and Elsberry, 1989; Carr and Elsberry, 1990; Wang and Li, 1992; Wang and Holland, 1996a). The steering flow is usually calculated over a certain radius from the tropical cyclone center in the horizontal and a deep pressure layer in the vertical (Dong and Neumann, 1986; Velden and Leslie, 1991; Franklin et al., 1996). For convenience, here we call it the conventional steering flow. As a rule of thumb, the conventional steering flow has been extensively used in tropical cyclone track forecasting and understanding of tropical cyclone motion (e.g., Simpson, 1948; Riehl and Burgner, 1950; Chan and Gray, 1982; Fiorino and Elsberry, 1989; Neumann, 1993; Wu and Emanuel, 1995a, b; Wang and Holland, 1996b, c; Wu et al., 2011a, b). Given complicated interactions between tropical cyclone circulation and its environment, tropical cyclone motion should not be like a leaf being steered only by the currents in the stream. Therefore, two fundamental issues still remain regarding the steering principle. First, why can the conventional steering play a dominant role in tropical cyclone motion? Second, when may tropical cyclone motion deviate considerably from the conventional steering?

The potential vorticity tendency (PVT) paradigm for tropical cyclone motion was proposed by Wu and Wang (2000), in which a tropical cyclone tends to move to the region of the PVT maximum. In other words, tropical cyclone motion is completely determined by the azimuthal wave-number-one component of PVT, and all of the factors that contribute to the azimuthal wave-number-one component of PVT play a potential role in tropical cyclone motion. The contributions of individual factors can be quantified through the PVT diagnosis, and the steering effect is one of the factors (Wu and Wang, 2000). Wu and Wang (2000, 2001a) evaluated the PVT approach using the output of idealized numerical experiments with a coarse spacing of 25 km and understood the vertical coupling of tropical cyclone circulation under the influence of vertical wind shear. Wu and Wang (2001b) found that convective heating can affect tropical cyclone motion by the heating-induced flow and the positive PVT that is directly generated by convective heating.

The PVT paradigm was further verified by Chan et al. (2002). The observational analysis indicated that the potential vorticity advection process is generally dominant in tropical cyclone motion without much change in direction or speed, while the contribution by diabatic heating (DH) is usually less important. An interesting finding of the study is that the contribution of diabatic heating becomes important for irregular tropical cyclone motion, suggesting that track oscillations as well as irregular track changes may be explained by changes in the convection pattern. The PVT approach has been used in understanding tropical cyclone motion in the presence of the effects of land surface friction (FR), river deltas, coastal lines, mountains, islands, cloud-radiative processes and sea surface pressure gradients (e.g., Wong and Chan, 2006; Yu et al., 2007; Fovell et al., 2010; Hsu et al., 2013; Wang et al., 2013; Choi et al., 2013).

As we know, the coarse resolution of the numerical experiment in Wu and Wang (2000) was unable to resolve the eyewall structure and tropical cyclone rainbands, which may affect tropical cyclone motion (Holland and Lander, 1993; Nolan et al., 2001; Oda et al., 2006; Hong and Chang, 2005). Under the PVT paradigm, in this study we use the output from a high-resolution numerical experiment to address the aforementioned two fundamental issues that are important to understanding tropical cyclone motion. The numerical experiment was conducted with the Advanced Research Weather Research and Forecast (WRF) model. In particular, an initially symmetric baroclinic vortex is embedded in the low-frequency atmospheric circulation of Typhoon Matsa (2005) to simulate tropical cyclone motion in a realistic large-scale environment. For simplicity, the present study focuses on the numerical experiment without the influences of land surface and topography.

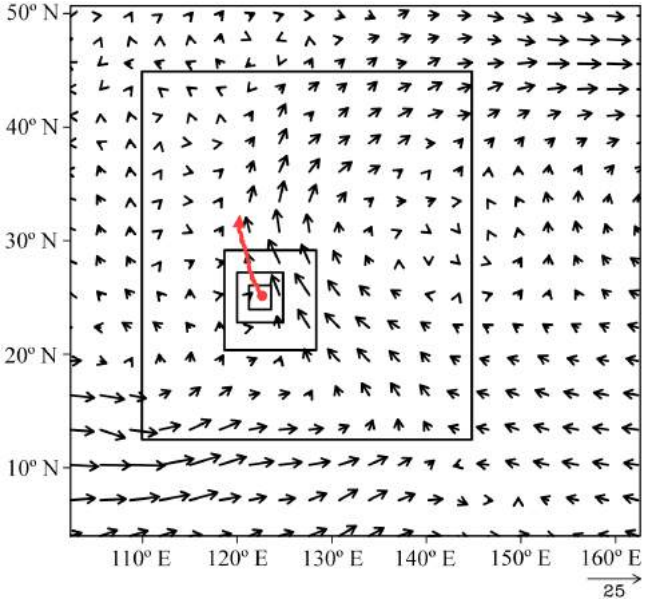

Figure 1. Model domains of the numerical experiment with the three innermost domains moving with the storm, the initial 850 hPa wind ($m\,s^{-1}$) field (vectors) and the simulated tropical cyclone track (red).

2 The output of the numerical experiment

The numerical experiment conducted with the WRF model (version 2.2) in this study contains a coarsest domain centered at 30.0° N, 132.5° E and four two-way interactive domains. In order to better simulate the tropical cyclone rainbands and eyewall structure, the horizontal resolutions are 27, 9, 3, 1 and 1/3 km. The three innermost domains move with the tropical cyclone (Fig. 1). The model consists of 40 vertical levels with a top at 50 hPa. The WRF single-moment three-class scheme and the Kain–Fritsch cumulus parameterization scheme (Kain and Fritsch, 1993) are used in the outermost domain. The WRF single-moment three-class scheme (Hong and Lim, 2006) and no cumulus parameterization scheme are used in the four inner domains. The other model physics options are the Rapid Radiative Transfer Model (RRTM) longwave radiation scheme (Mlaewe et al., 1997), the Dudhia shortwave radiation scheme (Dudhia, 1989) and the Yonsei University scheme for planetary boundary layer parameterization (Noh et al., 2003).

The National Centers for Environmental Prediction (NCEP) Final (FNL) Operational Global Analysis data with resolution of 1.0° × 1.0° every 6 h were used for deriving the large-scale background with a 20-day low-pass Lanczos filter (Duchon, 1979). The low-frequency fields were taken from those of Typhoon Matsa (2005) from 00:00 UTC on 5 August to 00:00 UTC on 9 August 2005. At 00:00 UTC on 5 August, the typhoon was located to the northeast of the island of Taiwan with a maximum surface wind of 45 $m\,s^{-1}$.

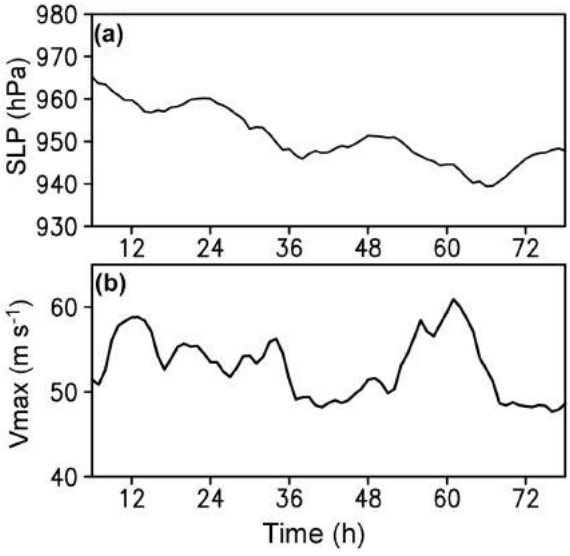

Figure 2. Time series of tropical cyclone intensity: **(a)** sea level minimum pressure (hPa) and **(b)** maximum wind speed at 10 m ($m\,s^{-1}$).

During the following 3 days, Matsa moved northwestward in the monsoon trough and made landfall on mainland China at 19:40 UTC on 5 August. The sea surface temperature is spatially uniform, being 29 °C. The analysis nudging for the wind components above the lower boundary layer is used in the coarsest domain to maintain the large-scale patterns with a nudging coefficient of $1.5 \times 10^{-4}\,s^{-1}$.

A symmetric vortex is initially embedded at 25.4° N, 123.0° E (Matsa's center) in the background (Fig. 1). The vortex was spun up for 18 h on an f plane without environmental flows to make it relatively consistent with the WRF model dynamics and physics. Considering several hours of the initial spin-up, here we focus only on the 72 h period from 6 to 78 h with the output at 1 h intervals. The simulated tropical cyclone takes a north-northwest track (Fig. 1), generally similar to that of Typhoon Matsa (2005). The evolution of tropical cyclone intensity is shown in Fig. 2. Although the sea level minimum pressure generally decreases with time, the maximum wind speed shows considerable fluctuations.

Figure 3 shows the simulated wind and radar reflectivity fields at 700 hPa. The vertical wind shear, which is calculated between 200 and 850 hPa over a radius of 500 km from the tropical cyclone center, is also plotted in the figure. The tropical cyclone center is defined as the geometric center of the circle on which the azimuthal mean tangential wind speed reaches a maximum (Wu et al., 2006). We use a variational method to determine the tropical cyclone center each hour at each level. Different definitions of the tropical cyclone center are also used, and it is found that fluctuations in tropical cyclone translation do not depend on the specific definition of the tropical cyclone center. At 24 h (Fig. 3a), the vertical wind shear is more than $10\,m\,s^{-1}$. The eyewall is open to the southwest, and strong eyewall convection occurs mainly on the downshear left side (Frank and Ritchie, 2001). The rainbands simulated in the innermost domain exhibit apparent cellular structures (Houze, 2010), mostly on the eastern side. The eyewall replacement cycle (ERC), which is important for tropical cyclone intensity change (Wu et al., 2012; Huang et al., 2012), is simulated in this numerical experiment. At 48 h (Fig. 3b), the vertical wind shear is weaker and the tropical cyclone undergoes an ERC. At 72 h (Fig. 3c), the outer eyewall just forms, while the inner one is breaking during the second ERC. Figure 3 suggests that the simulated tropical cyclone has a structure similar to a typical observed one, especially in the inner-core region.

Two eyewall replacement processes, which may affect tropical cyclone motion (Oda et al., 2006; Hong and Chang, 2005), can be further shown in Fig. 4. The evolution of the azimuthal mean component of the 700 hPa wind in the 9 km domain indicates the eyewall replacement processes around 42 and 68 h. During the first eyewall replacement, for example, the wind starts to intensify outside the eyewall around 36 h, in agreement with previous numerical studies (Wu et al., 2012; Huang et al., 2012). The radius of maximum wind is located about 40 km after the 6 h spin-up and decreases to about 30 km at 42 h. The lifetime maximum wind speed occurs at 60 h after the second eyewall replacement process (Fig. 2b). We also conducted a similar sensitivity experiment without the sub-kilometer domain. The tropical cyclone track in the experiment is generally similar to that in the sub-kilometer simulation, but no eyewall replacement cycle can be observed in the sensitivity experiment.

3 Dominant role of the conventional steering

The relationship between PVT and tropical cyclone motion can be written as (Wu and Wang, 2000)

$$\left(\frac{\partial P_1}{\partial t}\right)_f = \left(\frac{\partial P_1}{\partial t}\right)_m - C \times \nabla P_s, \quad (1)$$

where subscripts m and f indicate, respectively, the moving and fixed reference frames, and C is the velocity of the reference frame that moves with the tropical cyclone. In other words, C is the velocity of tropical cyclone motion, which can vary in the vertical. P_1 and P_s are the azimuthal wave-number-one and symmetric components of potential vorticity with respect to the storm center. It can be seen that the PVT generated in the fixed reference frame (the term on the left-hand side) is provided for the development of the wave-number-one component (the first term on the right-hand side) and for tropical cyclone motion (the second term on the right-hand side). The first term on the right-hand side of Eq. (1) was neglected in Wu and Wang (2000), but we retain it in this study. The term can be calculated with the 2 h change of the wave-number-one component in the frame that moves with the tropical cyclone center.

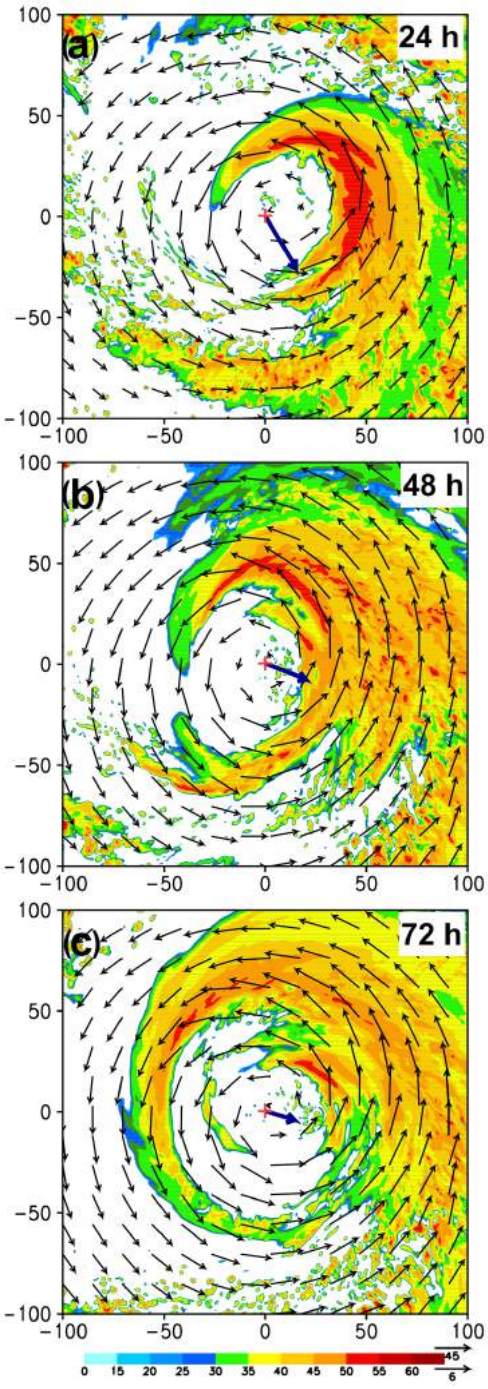

Figure 3. Simulated wind (vectors, m s^{-1}), radar reflectivity (shading, dBz) fields at 700 hPa, and the vertical wind shear (bold arrows in the center) between 200 and 850 hPa after **(a)** 24, **(b)** 48 and **(c)** 72 h integration. The x and y axes indicate the distance (km) relative to the storm center. The upper (lower) scale vector at the right lower corner is for the 700 hPa wind (vertical wind shear).

The PVT generated in the fixed reference frame can be calculated with the PVT equation in p coordinates as

$$\frac{\partial P}{\partial t} = -V \times \nabla P - \omega \frac{\partial P}{\partial p} - g \nabla_3 \times \left(-\frac{Q}{C_p \pi} q + \nabla\theta \times F \right), \quad (2)$$

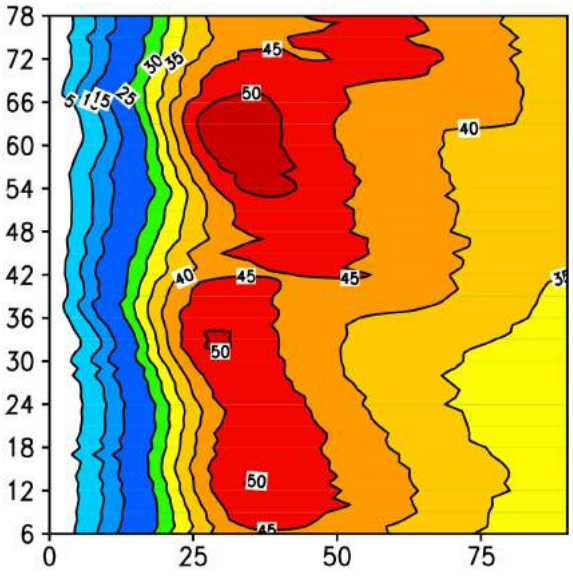

Figure 4. Evolution of the simulated azimuthal mean component (m s^{-1}) of the 700 hPa wind in the 9 km domain. The x axis and y axis indicate the distance (km) from the storm center and the integration time (hours), respectively.

where P, V and ω are potential vorticity, horizontal and vertical components of the wind velocity, respectively. Equation (2) contains horizontal advection (HA), vertical advection (VA), DH and FR terms on the right-hand side. Q, θ, q and F are diabatic heating rate, potential temperature, absolute vorticity and friction, while g, c_p and π are the gravitational acceleration, the specific heat of dry air at constant pressure and the Exner function, respectively. ∇_3 and ∇ denote the three- and two-dimensional gradient operators, respectively.

Following Wu and Wang (2000), a least-squares method is used to estimate the velocity of tropical cyclone motion (C) in Eq. (1). The translation velocity is also calculated with the hourly positions of the tropical cyclone center. For convenience, the tropical cyclone motion estimated with the PVT diagnostic approach and that with the center position are referred to as the PVT velocity and the tropical cyclone velocity, respectively, in the following discussion. In the PVT approach, we find that the estimated tropical cyclone motion is not very sensitive to the size of the calculation domain. As we know, however, determination of the conventional steering flow for a given tropical cyclone is not unique and depends on the size of the calculation domain (Wang et al., 1998). Here we select the calculation domain to minimize the difference between the tropical cyclone speed and the conventional steering flow. After a series of tests, we find that such a minimum can be reached when the 270 km radius is used. This is consistent with the analysis of the airborne Doppler radar data in Marks et al. (1992) and Franklin et al. (1996). The analysis indicated that tropical cyclone motion was best

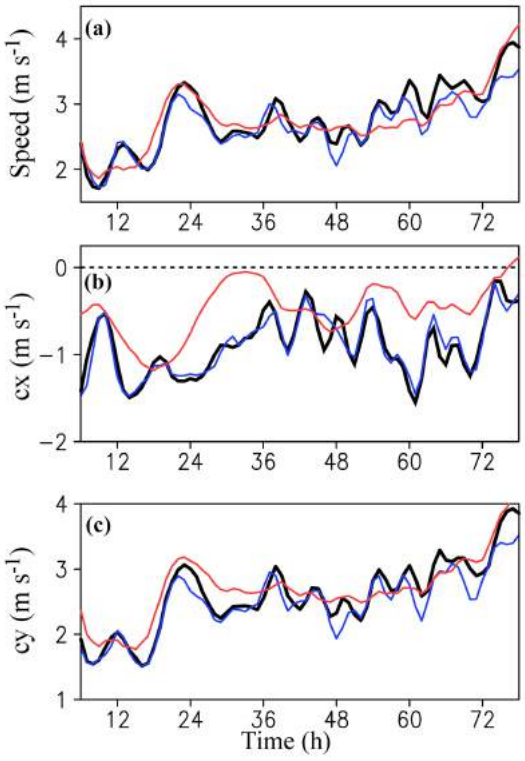

Figure 5. Time series of tropical cyclone speed (thick black), PVT speed (blue) and conventional steering (red): **(a)** magnitude, **(b)** zonal component and **(c)** meridional component.

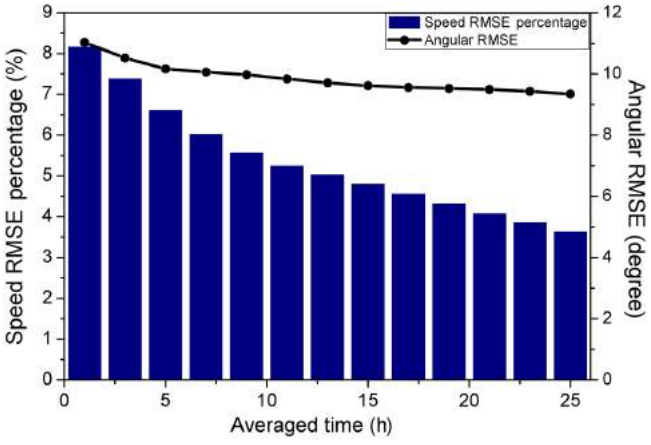

Figure 6. Changes of the RMSEs of the speed (blue boxes, %) and direction (black dots, °) of the conventional steering averaged over various time periods.

correlated with the depth-mean flow averaged over the inner region within 3° latitudes. Note that the PVT, tropical cyclone and steering velocities are calculated at each level, and then the depth-mean ones are averaged over the layer between 850 and 300 hPa.

Figure 5a shows the time series of the magnitudes of the tropical cyclone velocity (black), the PVT velocity (blue) and the conventional steering (red). Note that the PVT velocity and the conventional steering are instantaneous, whereas the tropical cyclone velocity is calculated based on the 2 h difference of the center position. For consistency, a three-point running mean is applied to the PVT speed and the conventional steering. These magnitudes generally increase as the tropical cyclone takes a north-northwest track. The mean speeds calculated from the PVT approach and the center positions are 2.86 and 2.75 m s^{-1} over the 72 h period. Compared to the tropical cyclone speed, the root-mean-square error (RMSE) of the PVT speed is 0.22 m s^{-1}, only accounting for 8 % of the tropical cyclone speed.

Figure 5b and c further display the zonal and meridional components of the tropical cyclone velocity (black), the PVT velocity (blue) and the conventional steering (red). While the westward component fluctuates about the mean zonal tropical cyclone (PVT) speed of -1.0 m s^{-1}, the northward component generally increases with time. Figure 5 clearly indicates that the translation velocity of the tropical cyclone can be well estimated with the PVT approach.

The environmental and secondary steering flows are indistinctly referred to as the conventional steering flow in this study. The conventional steering shown in Fig. 5 is averaged over the same radius (270 km) and the 850–300 hPa layer, as used in the calculation of the PVT speed. The 72 h mean magnitudes of the tropical cyclone velocity and the conventional steering are 2.86 and 2.87 m s^{-1}, respectively, only with a difference of 6.7° in the motion direction. We also calculated the RMSE of the conventional steering averaged over various time periods with the tropical cyclone speed (Fig. 6). The RMSE of the magnitude decreases with the increasing average period, generally less than 9 % of the translation speed of the tropical cyclone. The difference in direction also decreases with the increasing average period within 9–11°. Considering uncertainties in determining tropical cyclone centers and calculating the steering, we conclude that the conventional steering plays a dominant role in tropical cyclone motion. However, Fig. 5 indicates that the instantaneous tropical cyclone motion can considerably deviate from the conventional steering. The conventional steering cannot account for the fluctuations in tropical cyclone motion, which will be further discussed in Sect. 5.

4 Contributions of individual processes

The individual contributions of various terms in the PVT equation to tropical cyclone motion can also be estimated with Eq. (1), as shown by Wu and Wang (2000). In this study, the contribution of the FR term is calculated as the residual of the PVT equation. Figure 7 shows the individual contributions of the terms in the PVT equation to tropical cyclone motion. While the contribution of the HA term plays a dominant role (Fig. 7c), the figure exhibits considerable fluctu-

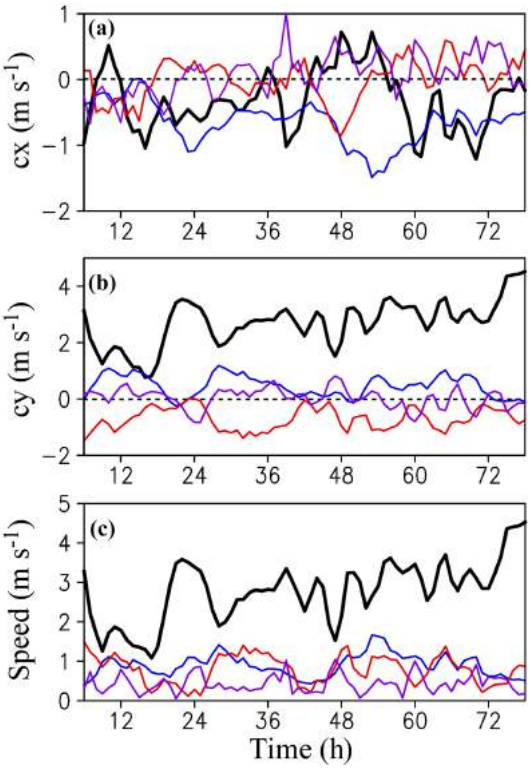

Figure 7. Contributions of the horizontal advection (HA, black), vertical advection (VA, blue), diabatic heating (DH, red) and friction (FR, purple) terms in the PVT equation to tropical cyclone motion: **(a)** zonal component, **(b)** meridional component and **(c)** magnitude.

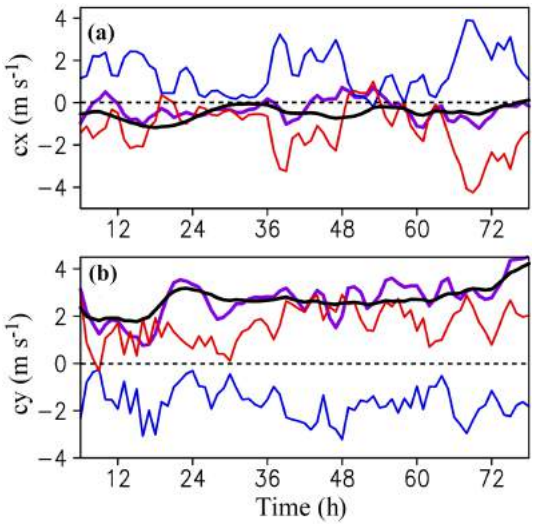

Figure 8. Time series of the conventional steering (thick black) and the contributions of the HA (thick purple), HA1 (red) and HA2 (blue) terms: **(a)** zonal component and **(b)** meridional component. Note that the conventional steering is deducted from the contribution of the HA1 term.

ations, suggesting that the contributions of the DH and VA terms tend to cancel each other (Fig. 7a and b). Here we discuss the contribution of each term in the PVT equation to understand the dominant role of the conventional steering in tropical cyclone motion.

4.1 Horizontal advection

As discussed in Wu and Wang (2001b), the HA term in the PVT equation can be approximately written as $V_1 \times \nabla P_s - V_s \times \nabla P_1$, where V_s is the symmetric component of the tangential wind and V_1 is the wave-number-one component of the asymmetric wind. The first term (HA1) represents the advection of the symmetric potential vorticity component by the asymmetric flow. The second term is the advection of the wave-number-one potential vorticity component by the symmetric flow (HA2).

The contribution of the HA1 term is literally the steering effect, but it is not the conventional steering that is calculated as the velocity of the mean wind averaged over 300–850 hPa within the radius of 270 km from the tropical cyclone center in this study. Wu and Wang (2001a) pointed out that the steering effect in the HA1 term is associated also with the gradient of the symmetric potential vorticity component, which makes its contribution confined to the inner region of tropical cyclones.

Figure 8 shows the contributions of the HA1 and HA2 terms, which exhibit considerable fluctuations with time. The contribution of HA and the conventional steering are also plotted. For clarity, the conventional steering is removed from the contribution of HA1 (i.e., HA1′). The 72 h mean difference between the contribution of HA1 and the conventional steering is $-1.25\,\mathrm{m\,s^{-1}}$ in the zonal component and $1.62\,\mathrm{m\,s^{-1}}$ in the meridional component, suggesting that the contribution of the HA1 term is considerably different from the conventional steering. In fact, the contributions of the HA1 and HA2 terms are highly anticorrelated. The correlations for the zonal and meridional components are -0.82 and -0.80, respectively. The negative correlations suggest the cancellation between the contributions of the HA1 and HA2 terms. As a result, the combined effect of the HA1 and HA2 terms can actually account for the effect of the conventional steering except the short-time fluctuations, as shown in Fig. 8. It is interesting to note that the contributions of the HA1 and HA2 terms increase in magnitude during the two eyewall replacement processes around 42 and 68 h, suggesting that the tropical cyclone motion considerably deviates from the steering of the asymmetric flow during eyewall replacement. However, it seems that the two eyewall replacement processes have little influence on the tropical cyclone motion (Fig. 5a).

The cancellation between the contributions of the HA1 and HA2 terms arises from the interaction between the symmetric and wave-number-one components of the tropical cyclone circulation. As an example, Fig. 9a shows HA1 and the wave-

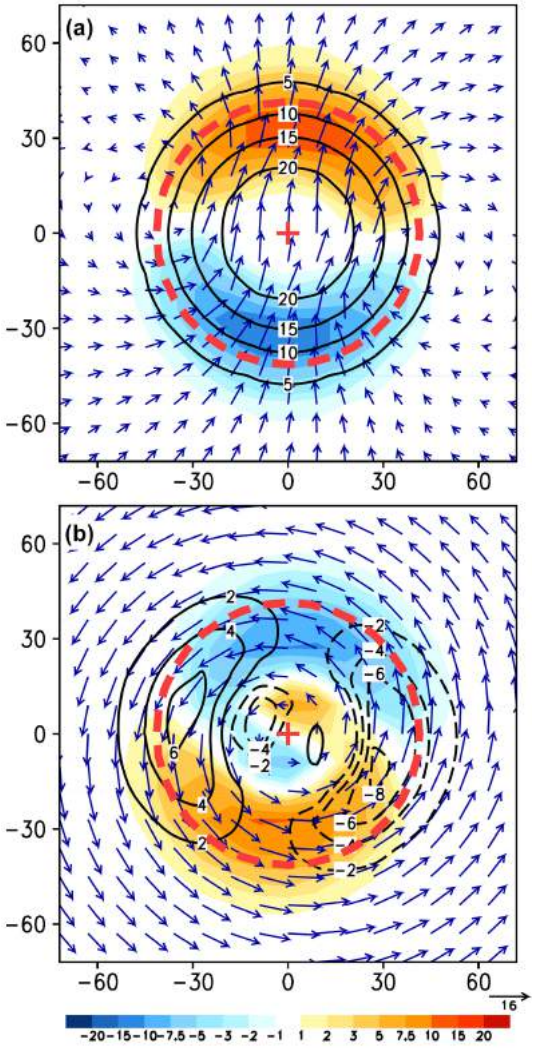

Figure 9. **(a)** HA1 (shaded, $10^{-10}\,m^2\,s^{-2}\,K\,kg^{-1}$) and **(b)** HA2 (shaded, $10^{-10}\,m^2\,s^{-2}\,K\,kg^{-1}$) with the wave-number-one and symmetric components of potential vorticity (contours, $10^{-6}\,m^2\,s^{-1}\,K\,kg^{-1}$) and winds (vectors, $m\,s^{-1}$) at 700 hPa after 18 h of integration. The dashed circle indicates the radius of maximum wind.

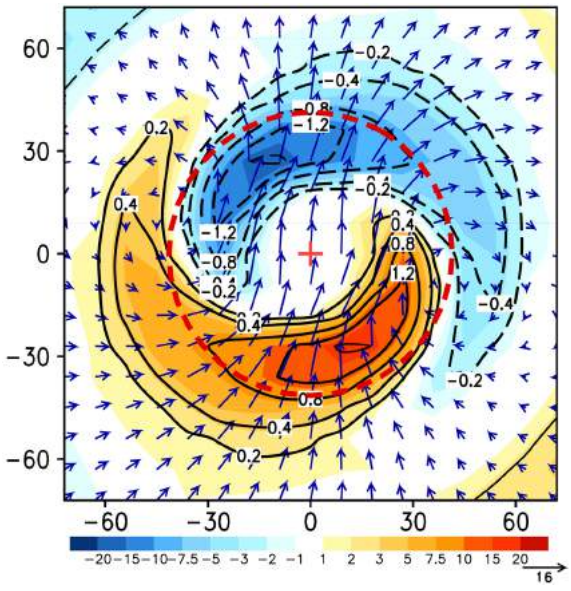

Figure 10. The wave-number-one components of the 500 hPa vertical motion (contours, $m\,s^{-1}$), 700 hPa winds relative to the tropical cyclone motion (vectors, $m\,s^{-1}$) and 500 hPa heating rate (shaded, $10^{-4}\,K\,s^{-1}$) after 18 h of integration. The dashed circle indicates the radius of maximum wind.

number-one components of potential vorticity (contours) and winds at 700 hPa after 18 h of integration. The positive (negative) anomalies of potential vorticity are nearly collocated with the cyclonic (anticyclonic) circulation. Since the potential vorticity in the inner core is generally elevated, the advection of the symmetric potential vorticity component by the flows between the cyclonic and anticyclonic circulations leads to the maximum (minimum) HA1 in the exit (entrance) of the flows between the cyclonic and anticyclonic circulation. On the other hand, the advection of the wave-number-one component of potential vorticity by the symmetric cyclonic flow leads to the maximum HA2 in the entrance and the minimum HA1 in the exit (Fig. 9b). Although the contributions of the HA1 and HA2 terms can fluctuate with a magnitude of about $4\,m\,s^{-1}$ (Fig. 8), their combined effect shows only small-amplitude fluctuations in the tropical cyclone motion. The short-time fluctuations will be discussed in the next section.

4.2 Contributions of diabatic heating and vertical advection

Some individual contributions in Fig. 7a and b are statistically correlated. For example, the zonal contribution of the HA term is negatively correlated with that of the DH term with a coefficient of −0.44, and the meridional contribution of the HA term is negatively correlated with that of the VA terms with a coefficient of −0.54. The correlation coefficients pass the significance test at the 95 % confidence level. It is suggested that the contributions of individual terms can partially cancel each other due to the coherent structure of the tropical cyclone.

We first discuss the contribution of the VA term. The VA contains two primary terms: the advection of the symmetric component of potential vorticity by the wave-number-one component of vertical motion (VA1) and wave-number-one component of potential vorticity by the symmetric component of vertical motion (VA2). Our examination indicates that the contribution of the VA term is dominated by that of VA1. That is, the direction of the contribution of the VA term is determined by the orientation of the wave-number-one component of vertical motion. Figure 10 shows the wave-number-

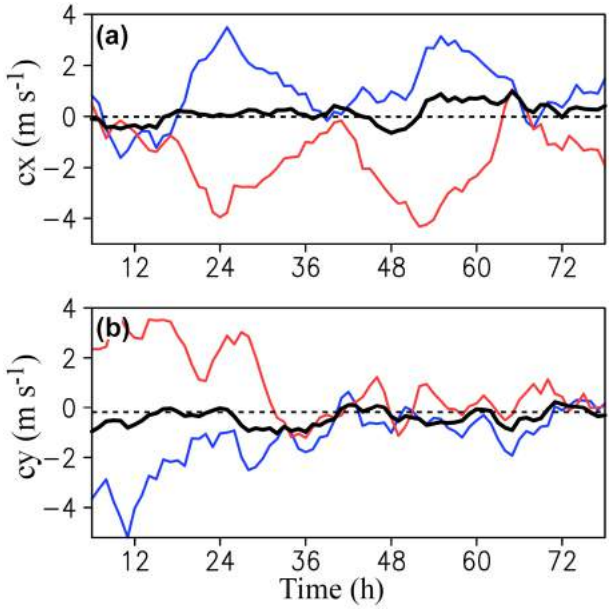

Figure 11. Time series of the contributions of diabatic heating at 700 (blue) and 400 hPa (red), and the contribution of diabatic heating (thick black) averaged over the layer between 300 and 850 hPa.

one components of the 500 hPa vertical motion, 700 hPa winds relative to tropical cyclone motion and 500 hPa heating rate after 18 h of integration. We can see that the upward (downward) motion generally occurs in the entrance (exit) region of the 700 hPa winds. Bender (1997) found that vorticity stretching and compression are closely associated with the vorticity advection due to the relative flow (difference between the wave-number-one flow and the TC motion), but Riemer (2016) recently argued that Bender's mechanism did not work in his idealized experiment. We find that the contribution of the HA term is indeed significantly correlated with those of the VA and DH terms, suggesting the relationship between the vertical motion (diabatic heating) and the relative flow.

The contribution of diabatic heating results mainly from $-q_s \times \nabla_3 h_1$, where q_s is the symmetric component of the absolute vorticity, ∇_3 the three-dimensional gradient operator and h_1 the wave-number-one component of diabatic heating rate. Since the absolute vorticity is dominated by the vertical component of relative vorticity and diabatic heating rate reaches its maximum in the middle troposphere, it is conceivable that the contribution of diabatic heating should cancel each other in the low and upper troposphere. Figure 11 shows the contribution of diabatic heating at 700 and 400 hPa. The correlation between 700 and 400 hPa is −0.68 in the zonal direction and −0.67 in the meridional direction.

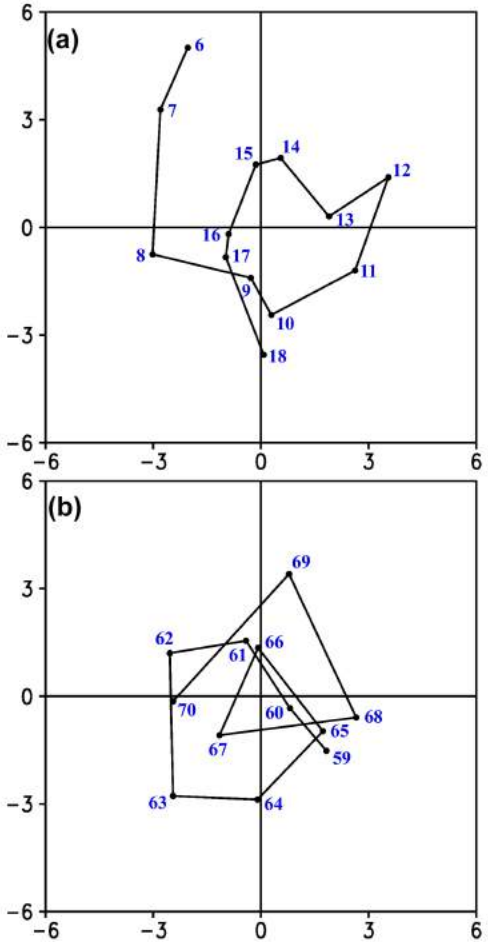

Figure 12. Small-amplitude oscillation of the tropical cyclone track with respect to the 9 h running mean track: **(a)** 6–18 and **(b)** 59–69 h. The x and y axes indicate the distance (km) relative to the 9 h running mean track.

5 Trochoidal motion

As shown in Fig. 5, the tropical cyclone motion exhibits considerable fluctuations. In an instant, the steering can significantly deviate from the tropical cyclone motion. At 60 h, for example, the zonal steering is $-0.55\ \mathrm{m\ s^{-1}}$, about one-third of the zonal motion of the tropical cyclone ($-1.42\ \mathrm{m\ s^{-1}}$); the meridional steering is $2.71\ \mathrm{m\ s^{-1}}$, slower than the meridional motion of the tropical cyclone ($3.05\ \mathrm{m\ s^{-1}}$). The deviation from the tropical cyclone motion is 13.5° in the direction and 18 % in the magnitude.

Based on radar data and satellite images, many studies have documented the oscillation of a tropical cyclone track with respect to its mean motion vector (e.g., Jordan and Stowell, 1955; Lawrence and Mayfield, 1977; Muramatsu, 1986; Itano et al., 2002; Hong and Chang, 2005). The periods of track oscillations range from less than an hour to a few days (Holland and Lander, 1993). In this study, the small-

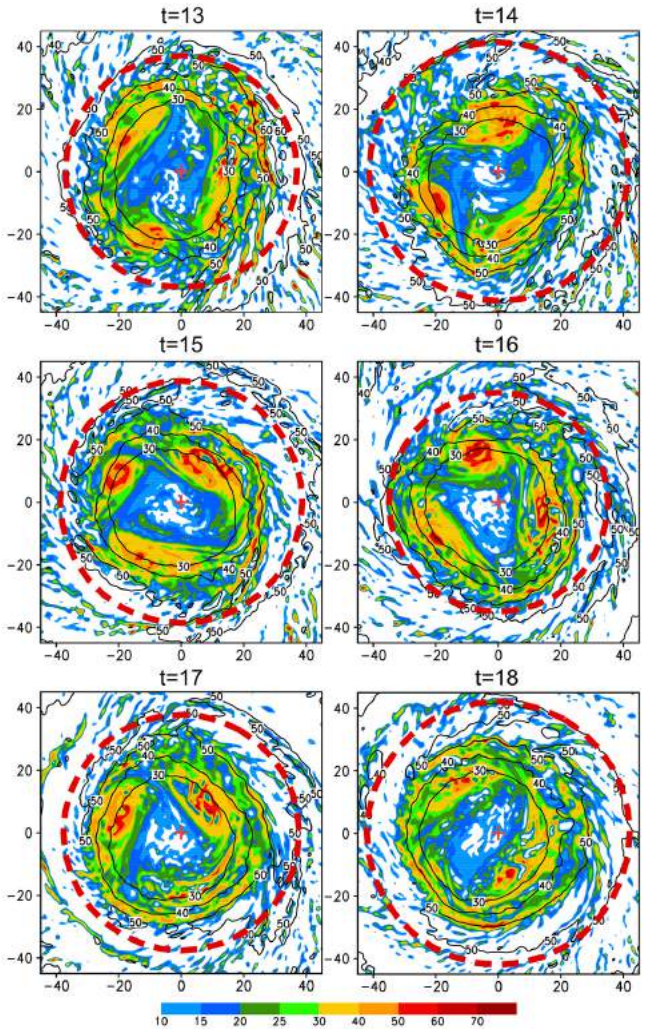

Figure 13. Distribution of potential vorticity (shaded, $10^{-6}\,m^2\,s^{-1}\,K\,kg^{-1}$) and magnitude of wind (contour, $m\,s^{-1}$) within the inner-core region during the period of 13–18 h at 700 hPa. The dashed circle shows the radius of maximum wind, with the tropical cyclone center indicating with crosses.

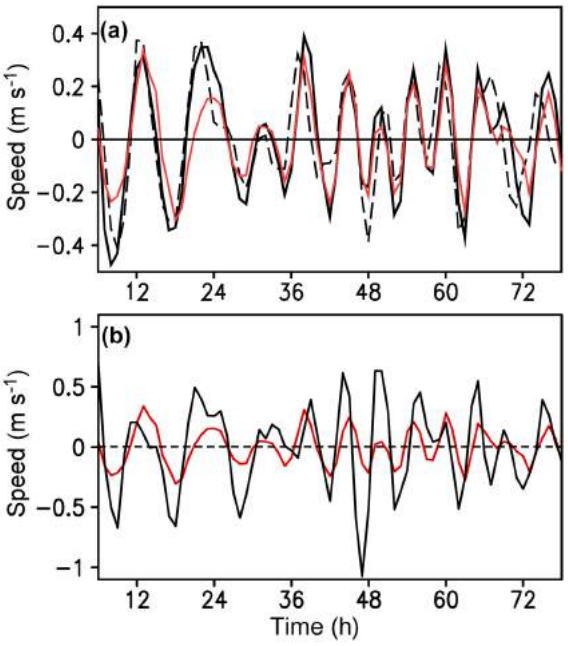

Figure 14. Fluctuations (deviation from the 9 h running mean) of **(a)** the tropical cyclone speed (black solid), the PVT speed (black dashed) and the difference between the tropical cyclone speed and the conventional steering (red solid), and **(b)** the difference between the tropical cyclone speed and the conventional steering (red solid), and the difference between the contribution of the HA term and the conventional steering (black).

scale oscillation with amplitudes comparable to the eye size and periods of several hours is referred to as the trochoidal motion of the tropical cyclone center. Willoughby (1988) showed that a pair of rotating mass and sink source could lead to trochoidal motion with periods ranging from 2 to 10 h. Flatau and Stevens (1993) argued that wave-number-one instabilities in the outflow layer of tropical cyclones could cause trochoidal motion. Nolan et al. (2001) found that the small-amplitude trochoidal motion is associated with the instability of the wave-number-one component of tropical cyclone circulation due to the presence of the low-vorticity eye. The instability in their three-dimensional simulation with a baroclinic vortex quickly led to substantial inner-core vorticity redistribution and mixing, displacing the vortex center that rotates around the vortex core. Our spectral analysis indicates two peaks of the fluctuations of the tropical cyclone motion centered at 5 and 9 h (figure not shown), suggesting that the trochoidal motion is simulated in our high-resolution numerical simulation.

Figure 12 shows the oscillation of the tropical cyclone track with respect to the 9 h running mean track for the periods 6–18 and 59–70 h. We can see that the displacement from the mean track is usually less than 6 km with a period of several hours in this study. This displacement is less than the size of the tropical cyclone eye. In general, the tropical cyclone center rotates cyclonically relative to the mean track position, in agreement with previous observational and numerical studies (Lawrenece and Mayfield, 1977; Muramatsu, 1986; Itano et al., 2002; Willoughby, 1988; Nolan et al., 2001). In association with the trochoidal motion of the tropical cyclone center, as suggested by Nolan et al. (2001), substantial potential vorticity redistribution and mixing can be observed in the inner-core region (Fig. 13). During the period of 13–18 h, the tropical cyclone eye generally looks like a triangle, but the orientation of the triangle changes rapidly, suggesting the potential vorticity redistribution and mixing in the eye.

The trochoidal motion is well indicated in the translation speed estimated with the PVT approach. Figure 14a shows the fluctuations of tropical cyclone speed, the PVT speed, and the difference between the tropical cyclone speed and

the conventional steering, in which the 9 h running mean has been removed. We can see that the fluctuations of tropical cyclone motion are well represented in the PVT speed. Moreover, the consistency between the fluctuations of tropical cyclone motion and those with the conventional steering removed suggests that the small-amplitude oscillation of the tropical cyclone motion cannot be accounted for by the conventional steering. Figure 14b further compares the time series of tropical cyclone motion relative to the conventional steering with the time series of the contribution of the HA term relative to the conventional steering. The two time series are correlated with a coefficient of 0.60. We can see that the contribution of the HA term plays an important role in the fluctuations. Since the non-steering effect can well account for the fluctuations (Fig. 14a), Fig. 14b suggests that the VA and DH tend to reduce the magnitude of the fluctuations.

6 Summary

In this study, we addressed two fundamental questions regarding the steering principle that has been widely applied to tropical cyclone forecasting and research for about a century (Fujiwara and Sekiguchi, 1919; Bowie, 1922). One is why the conventional steering plays a dominant role in tropical cyclone motion, and the other is when tropical cyclone motion deviates considerably from the steering. The PVT diagnosis approach proposed by Wu and Wang (2000) is used with the output from a high-resolution numerical experiment. It is found that the PVT approach can well estimate tropical cyclone motion, including the small-amplitude trochoidal motion relative to the mean tropical cyclone track.

The effect of the conventional steering flow that is averaged over a certain radius from the tropical cyclone center and a deep pressure layer (e.g., 850–300 hPa) actually represents the combined contribution from both the advection of the symmetric potential vorticity component by the asymmetric flow (HA1) and the advection of the wave-number-one potential vorticity component by the symmetric flow (HA2), although the contribution of the HA1 term is literally the effect of steering (Wu and Wang, 2001a, b). The conventional steering generally plays a dominant role in tropical cyclone motion since the contributions from other processes are largely cancelled out due to the coherent structure of tropical cyclone circulation.

The trochoidal motion of the tropical cyclone center is simulated in the numerical experiment with amplitudes smaller than the eye radius and periods of several hours. The tropical cyclone center rotates cyclonically around the mean track, in agreement with previous observational and numerical studies (Lawrenece and Mayfield, 1977; Muramatsu, 1986; Itano et al., 2002; Willoughby, 1988; Nolan et al., 2001). It is found that the small-amplitude trochoidal motion cannot be accounted for by the effect of the conventional steering, although the contribution of the HA term plays an important role in the fluctuations. In agreement with previous studies (Willoughby, 1988; Nolan et al., 2001), we suggest that the small-amplitude trochoidal motion results from the asymmetric dynamics of the tropical cyclone inner core. It is also found that the instantaneous speed of tropical cyclone motion can considerably deviate from the conventional steering, while the latter better represents tropical cyclone motion when averaged over a reasonable time period.

7 Data availability

The underlying research data were the output of a numerical experiment and available on request by contacting the first author.

Acknowledgements. Many thanks go to Christopher W. Landsea of the National Hurricane Center for providing us the early references on the steering principle. This research was jointly supported by the National Basic Research Program of China (2013CB430103, 2015CB452803), the National Natural Science Foundation of China (grant no. 41275093) and the project of the specially appointed professorship of Jiangsu Province. We appreciate C.-C. Wu and two anonymous reviewers for their constructive comments.

Edited by: H. Wernli
Reviewed by: C.-C. Wu and two anonymous referees

References

Bender, M. A.: The effect of relative flow on the asymmetric structure in the interior of hurricanes, J. Atmos. Sci., 54, 703–724, 1997.

Bowie, E. H.: Formation and movement of West Indian hurricanes. Mon. Weather Rev., 50, 173-179, 1922.

Carr, L. E. and Elsberry, R. L.: Observational evidence for predictions of tropical cyclone propagation relative to steering, J. Atmos. Sci., 47, 542–546, 1990.

Chan, J. C.-L.: An observation al study of physical processes responsible for tropical cyclone motion, J. Atmos. Sci., 41, 1036–1048, 1984.

Chan, J. C.-L. and Gray, W. M.: Tropical cyclone motion and surrounding flow relationship, Mon. Weather Rev., 110, 1354–1374, 1982.

Chan, J. C-L. and Williams, R. T.: Analytical and numerical studies of beta-effect in tropical cyclone motion, Part I: Zero mean flow, J. Atmos. Sci., 44, 1257–1265, 1987.

Chan, J. C.-L., Ko, F. M. F., and Lei, Y. M.: Relationship between potential vorticiy tendency and tropical cyclone motion, J. Atmos. Sci., 59, 1317–1336, 2002.

Choi, Y., Yun, K.-S., Ha, K.-J., Kim, K.-Y., Yoon, S.-J., and Chan, J.-C.-L.: Effects of Asymmetric SST Distribution on Straight-Moving Typhoon Ewiniar (2006) and Recurving Typhoon Maemi (2003), Mon. Weather Rev., 141, 3950–3967, 2013.

Dong, K., and C. J. Neumann, 1986: The relationship between tropical cyclone motion and environmental geostrophic flows, Mon. Weather Rev., 114, 115–122, 1986.

Duchon, C. E.: Lanczos filtering in one and two dimensions, J. Appl. Meteor., 18, 1016–1022, 1979.

Dudhia, J.: Numerical study of convection observed during the winter monsoon experiment using a mesoscale two-dimensional model, J. Atmos. Sci., 46, 3077–3107, 1989.

Fiorino, M. and Elsberry, R. L.: Some aspects of vortex structure related to tropical cyclone motion, J. Atmos. Sci., 46, 975–990, 1989.

Flatau, M. and Stevens, D.: The Role of Outflow-Layer Instabilities in Tropical Cyclone Motion, J. Atmos. Sci., 50, 1721–1733, 1993.

Fovell, R. G., Corbosiero, K. L., Seifert, A., and Liou, K.-N.: Impact of cloud-radiative processes on hurricane track, Geophys. Res. Lett., 37, L07808, doi:10.1029/2010GL042691, 2010.

Frank, W. and Ritchie, E. A.: Effects of vertical wind shear on the intensity and structure of numerically simulated hurricanes, Mon. Weather Rev., 129, 2249–2269, 2001.

Franklin, J. L., Feuer, S. E., Kaplan, J., and Aberson, S. D.: Tropical cyclone motion and surrounding flow relationship: Searching for beta gyres in Omega dropwindsonde datasets, Mon. Weather Rev., 124, 64–84, 1996.

Fujiwhara, S. and K. Sekiguchi: Estimated 300 m isobars and the weather of Japan, J. Meteor. Soc. Japan, 38, 254–259, 1919 (in Japanese).

Holland, G. J.: Tropical cyclone motion: Environmental interaction plus a beta effect, J. Atmos. Sci., 40, 328–342, 1983.

Hong, S. Y. and Lim, J. O. J.: The WRF single-moment 6-class microphysics scheme (WSM6)[J], J. Korean Meteor. Soc., 42, 129–151, 2006.

Hong, J.-S. and Chang, P.-L.: The trochoid-like track in Typhoon Dujuan (2003), Geophys. Res. Lett., 32, L16801, doi:10.1029/2005GL023387, 2005.

Houze, R. A.: Clouds in tropical cyclones, Mon. Weather Rev., 138, 293–344, 2010.

Hsu, L.-H., Kuo, H.-C., and Fovell, R. G.: On the Geographic Asymmetry of Typhoon Translation Speed across the Mountainous Island of Taiwan, J. Atmos. Sci., 70, 1006–1022, 2013.

Huang, Y.-H., Montgomery, M. T., and Wu, C.-C.: Concentric eyewall formation in Typhoon Sinlaku (2008) – Part II: Axisymmetric dynamical processes, J. Atmos. Sci., 69, 662–674, 2012.

Itano, T., Naito, G., and Oda, M.: Analysis of elliptical eye of Typhoon Herb (T9609) (in Japanese with English abstract), Sci. Eng. Rep. Natl. Def. Acad., 39, 9–17, 2002.

Kain, J. S. and Fritch, J. M.: Convective parameterization for mesoscale models: the Kain-Fritch scheme. The representation of cumulus convection in numerical models, Meteorol. Monogr., 46, 165–170, 1993.

Lawrence, M. B. and Mayfield, B. M.: Satellite observations of trochoidal motion during Hurricane Belle 1976, Mon. Weather Rev., 105, 1458–1461, 1977.

Marks Jr., F. D., Houze Jr., R. A., and Gamache, J. F.: Dual-aircraft investigation of the inner core of Hurricane Norbert, Part I: Kinematic structure, J. Atmos. Sci., 49, 919–942, 1992.

Mlawer, E. J., Taobman, S. J., Brown, P. D., Iacono, M. J., and Clough, S. A.: Radiative transfer for inhomogeneous atmosphere: RRTM, a validated correlated-k model for the longwave, J. Geophys. Res., 102, 16663–16682, 1997.

Muramatsu, T.: Trochoidal motion of the eye of Typhoon 8019, J. Meteor. Soc. Japan, 64, 259–272, 1986.

Neumann, C. J.: Global overview, Global Guide to Tropical Cyclone Forecasting, World Meteor. Org., 1.1–1.56, 1993.

Noh, Y., Cheon, W. G., Hong, S.-Y., and Raasch, S.: Improvement of the K-profile model for the planetary boundary layer based on large eddy simulation data, Bound.-Layer Meteor., 107, 401–427, 2003.

Nolan, D. S., Montgomery, M. T., and Grasso, L. D.: The wavenumber-one instability and trochoidal motion of hurricane-like vortices, J. Atmos. Sci., 58, 3243–3270, 2001.

Oda, M., Nakanishi, M., and Naito, G.: Interaction of an Asymmetric Double Vortex and Trochoidal Motion of a Tropical Cyclone with the Concentric Eyewall Structure, J. Atmos. Sci., 63, 1069–1081, 2006.

Riehl, H., and Burgner, N. M.: Further studies on the movement and formation of hurricanes and their forecasting, Bull. Amer. Meteor. Soc., 31, 244–253, 1950.

Riemer, M.: Meso-β-scale environment for the stationary band cpmplex of verticall-sheared tropical cyclones, Q. J. R. Meteorol. Soc., 142, 2442–2451, 2016.

Simpson, R. H.: On the movement of tropical cyclones, Trans. Amer. Geophy. Union, 27, 641–655, 1946.

Velden, C. S. and Leslie, L. M.: The basic relationship between tropical cyclone intensity and the depth of the environmental steering layer in the Australian region, Weather Forecast., 6, 244–253, 1991.

Wang, B. and Li, X.: The beta drift of three-dimensional vortices: A numerical study, Mon. Weather Rev., 120, 579–593, 1992.

Wang, B., Elsberry, R. L., Wang, Y., and Wu, L.: Dynamics of tropical cyclone motion: A review, Sci. Atmos. Sin., 22, 1–12, 1998.

Wang, C.-C., Chen, Y.-H., Kuo, H.-C., and Huang, S.-Y.: Sensitivity of typhoon track to asymmetric latent heating/rainfall induced by Taiwan topography: A numerical study of Typhoon Fanapi (2010), J. Geophys. Res.-Atmos., 118, 3292–3308, 2013.

Wang, Y. and Holland, G. J.: The beta drift of baroclinic vortices, Part I: Adiabatic vortices, J. Atmos. Sci., 53, 411–427, 1996a.

Wang, Y. and Holland, G. J.: The beta drift of baroclinic vortices. Part II:Diabatic vortices, J. Atmos. Sci., 53, 3737–3756, 1996b.

Wang, Y. and Holland, G. J.: Tropical cyclone motion and evolution in vertical shear, J. Atmos. Sci., 53, 3313–3332, 1996c.

Willoughby, H.: Linear motion of a shallow-water, barotropic vortex, J. Atmos. Sci., 45, 1906–1928, 1988.

Wong, M. L. M. and Chan, J. C. L.: Tropical cyclone motion in response to land surface friction, J. Atmos. Sci., 63, 1324–1337, 2006.

Wu, C.-C. and Emanuel, K. A.: Potential vorticity diagnostics of hurricane movement, Part I: A case study of Hurricane Bob (1991), Mon. Weather Rev., 123, 69–92, 1995a.

Wu, C.-C. and Emanuel, K. A.: Potential vorticity diagnostics of hurricane movement, Part II: Tropical Storm Ana (1991) and Hurricane Andrew (1992), Mon. Weather Rev., 123, 93–109, 1995b.

Wu, C.-C., Huang, Y.-H., and Lien, G.-Y.: Concentric eyewall formation in Typhoon Sinlaku (2008) – Part I: Assimilation of T-PARC data based on the Ensemble Kalman Filter (EnKF), Mon. Weather Rev., 140, 506–527, 2012.

Wu, L. and Wang, B.: A potential vorticity tendency diagnostic approach for tropical cyclone motion, Mon. Weather Rev., 128, 1899–1911, 2000.

Wu, L. and Wang, B.: Movement and vertical coupling of adiabatic baroclinic tropical cyclones, J. Atmos. Sci., 58, 1801–1814, 2001a.

Wu, L. and Wang, B.: Effects of convective heating on movement and vertical coupling of tropical cyclones: A numerical study, J. Atmos. Sci., 58, 3639–3649, 2001b.

Wu, L., Braun, S. A., Halverson, J., and Heymsfield, G.: A numerical study of Hurricane Erin (2001), Part I: Model verification and storm evolution, J. Atmos. Sci., 63, 65–86, 2006.

Wu, L., Liang, J., and Wu, C.-C.: Monsoonal Influence on Typhoon Morakot (2009), Part I: Observational analysis, J. Atmos. Sci., 68, 2208–2221, 2011a.

Wu, L., Zong, H., and Liang, J.: Observational analysis of sudden tropical cyclone track changes in the vicinity of the East China Sea, J. Atmos. Sci., 68, 3012–3031, 2011b.

Yu, H., Huang, W., Duan, Y. H., Chan, J. C. L., Chen, P. Y., and Yu, R. L.: A simulation study on pre-landfall erratic track of typhoon Haitang (2005), Meteorol. Atmos. Phys., 97, 189–206, 2007.